Nanoscale

COMMUNICATION

View Article Online
View Journal | View Issue

Cite this: *Nanoscale*, 2015, **7**, 2301

Received 17th November 2014,
Accepted 5th January 2015

DOI: 10.1039/c4nr06785a

www.rsc.org/nanoscale

Conductance measurements of individual polypyrrole nanobelts

C. Hentschel,[a,b,c] L. Jiang,*[a] D. Ebeling,[d] J. C. Zhang,[a] X. D. Chen[e] and L. F. Chi*[a,b,c]

We present here a study on the electrical conduction properties of individual polypyrrole nanobelts by using conductive atomic force microscopy and discuss a general effect while probing soft materials. A length-dependent analysis demonstrates that the tip could induce local defects into the polymer structure and, thus diminishes the electrical conduction.

Accurate knowledge about surface/interface properties of micro- and nanometer scales is of great importance for the understanding of material properties and processes in different research areas. In this regard atomic force microscopy (AFM) has been developed as one of the most versatile standard tools for the characterization of surface structures in the last few decades,[1–3] especially for organic/polymeric soft materials.[4,5] The success of AFM is based on its experimental setup which offers the unique possibility to get direct access not only to, for example, topographical and mechanical information but also to other physical properties such as electric and magnetic properties. In this regard, the investigation of conductive one-dimensional (1D) nanostructures, especially the investigation of conductive polymer nanostructures, has become exceedingly attractive due to their high potential for optical and electrical applications in micro- and nanodevices.[6–18] Furthermore, 1D nanostructures have been reported to be promising candidates for efficient electron transport.[19,20]

Here, we present a length dependent analysis of individual conductive polypyrrole (Ppy) nanobelts with different widths, specifically in a sub-100 nm range, in order to characterize the electrical conductance by using AFM based conductivity measurements. In the current sensing AFM mode (C-AFM) an electrical conductive tip scans in mechanical contact over the surface of the sample of interest allowing one to measure the local resistance of the sample.[15,21,22] The conductive polymeric nanobelts used here are prepared on an insulating layer of SiO_2 with one end electrically connected to a gold electrode while the other end is free on the substrate. By applying a bias voltage between the tip and the sample and measuring the current with an external current amplifier, the local resistance of the sample surface can be analyzed as a function of the x,y-position of the tip. This enables a simultaneous recording of topographical and electrical information of the sample. In this setup the AFM tip works as a movable electrode sensing the axial electrical conduction through a single belt to the gold electrode.[21,23,24] An illustration of the electrical circuit used in these experiments is given in Fig. 1A.

Additionally, a typical AFM scan ($20 \times 20\ \mu m^2$) of the device that illustrates the simultaneously recorded topography (B) and current (C) images is shown. From these images single in-plane polymer belts are clearly distinguishable. A cross section perpendicular to the axis of the belts shows an average belt height of about 25 nm. Furthermore, the electrical conduction properties of single belts are clearly confirmable from the conductivity map. To quantify the conduction properties of single Ppy belts the measured current is analyzed as a function of the distance L to the electrode which designates the electron transport length through the Ppy belt.

Therefore, the current map (Fig. 2A) is studied by extracting the maximum current values of each scan line corresponding to the belt of interest. In the next step these current values are plotted *versus* the distance L as represented in Fig. 2B (top). As expected the graph reveals a trend of continuous decreasing current I with the length. To classify the conduction properties of the Ppy belt Ohm's law $R = U/I$ is used to convert the

[a]*Jiangsu Key Laboratory for Carbon-Based Functional Materials & Devices, Institute of Functional Nano & Soft Materials (FUNSOM) & Collaborative Innovation Center of Suzhou Nano Science and Technology, Soochow University, 199 Ren-Ai Road, Suzhou Jiangsu 215123, P. R. China. E-mail: ljiang@suda.edu.cn, chilf@suda.edu.cn*
[b]*Physikalisches Institut, Universität Münster, Wilhelm-Klemm-Str. 10, 48149 Münster, Germany*
[c]*Center for NanoTechnology (CeNTech), Heisenbergstraße 11, 48149 Münster, Germany*
[d]*Institute of Applied Physics (IAP), Justus-Liebig-Universität Giessen, Germany*
[e]*School of Materials Science and Engineering, Nanyang Technological University, 50 Nanyang Avenue, Singapore 639798, Singapore*

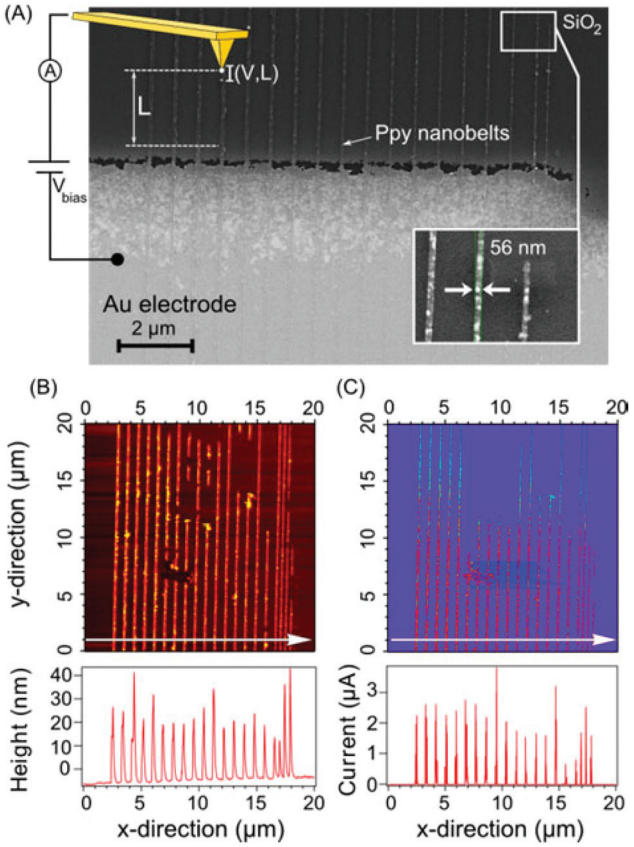

Fig. 1 Schematic setup of the electrical circuit used in the experiments. (A) SEM image of polymer nanobelts (vertical line structure) written on an insulating substrate of SiO_2 and electrically connected to a gold electrode (bottom, bright part). The white box displays the position of the enlarged section of the polymer belts which are used to determine the width of the belts. The schematic inset displays the experimental setup used: while applying a bias voltage *V* between a conductive AFM tip and sample, the local current *I* flowing through the nanobelts can be measured and analyzed as a function of its length *L*. Typical topography (B) and current (C) image (including the cross-sectional profiles) of the sample system obtained in C-AFM mode with an applied bias voltage of 1 V. The images reveal several interrupted polymer wires whose non-conductive parts are separated by gaps from conductive parts.

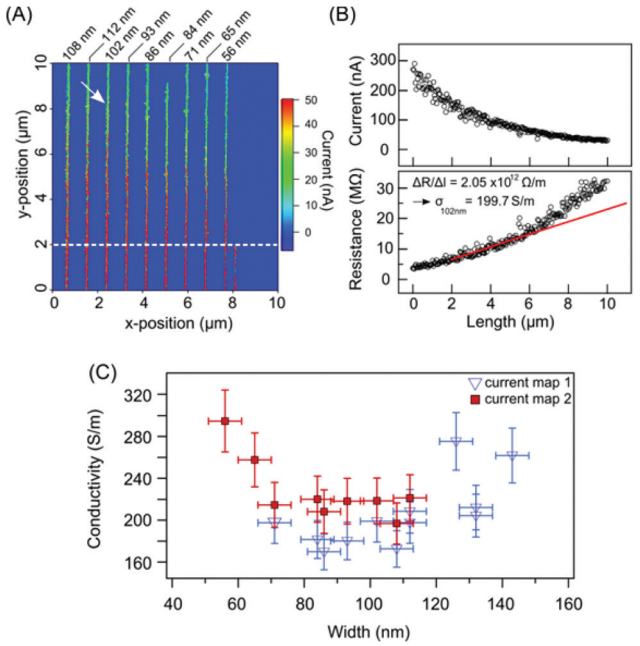

Fig. 2 (A) Typical conductivity map (10 × 10 μm^2) of Ppy belts on a SiO_2 substrate (bias voltage of 1 V). The measured width of the nanobelts decreases from 112 nm to 56 nm as indicated. All belts have an average height of 25 nm. (B) Local current, *I*, (top) and resistance, *R*, (bottom) *vs.* length of a single nanobelt. The local resistance was determined from the measured current data *via* Ohm's law. The line shows a linear fit to the resistance values in the range from 2 μm to 5 μm. The slope was used to determine the conductivity of the corresponding belt. (C) Calculated conductivities for polymer belts of different widths. The data were derived from two different adjoining current maps which show an overlap for the belts ranging from 71 nm to 112 nm. Current map 1 (blue open triangles): belt widths ranging from 71 nm to 143 nm; current map 2 (red closed squares): belt widths ranging from 56 nm to 112 nm.

measured current values into the corresponding local resistance values *R* (Fig. 2B, bottom). The conductivity σ of a metallic wire is determined by the relationship between the length and the resistance according to

$$\sigma = \frac{1}{A}\frac{\Delta L}{\Delta R} \quad (1)$$

where *A* is the cross-sectional area of the wire. In other words, the conductivity is inversely proportional to the slope of the resistance *versus* the length curve ($\sigma^{-1} \sim \Delta R/\Delta L$).

When fitting the slope of the resistance *vs.* length curves we restrict ourselves to a length range of 2 to 5 μm due to the following reasons: (1) in contrast to an ideally conducting metal the individual belts probed in this study exhibit a non-linear resistance *versus* length behaviour *R*(*L*) which indicates that the electron transport within the Ppy belts is driven by local defects inside the polymer and might be attributed to strong Anderson localization.[23] This non-linear effect becomes increasingly prominent when the length of the belts exceeds approx. 6 μm (see Fig. 2B, bottom). Due to this fact we limited ourselves to fitting the slope of the resistance *vs.* length curve only for length values smaller than 5 μm. (2) Based on the deposition method of the gold electrodes by using a shadow-mask thermal evaporation technique, the edges of the electrodes are not clearly defined. This may lead to a contamination of the polymer with Au particles after the Ppy growth and, consequently, to a distortion of the conduction behaviour within the belts. It has been reported that polymer–metal matrix composites show an enhanced conductivity.[25] For this reason we fit eqn (1) in a range starting from 2 μm away from the gold electrode as indicated in Fig. 2A (dashed, horizontal line, the Au electrode is located at the bottom part of the image outside the scan range).

By fitting the slope of the resistance *vs.* length curve, for instance, for the marked belt in Fig. 2A we can calculate a conductivity of (200 ± 20) S m^{-1}, with a width of 102 ± 5 nm and a uniform height of 25 nm. As noted, we applied the fit of eqn (1) in the nearly linear part ranging from 2 μm to 5 μm.

Fig. 2C displays the conductivities evaluated as described for all single nanobelts as a function of their widths ranging from 145 nm to 56 nm. The conductivities were derived from two adjoining current maps which show an overlap for the belts ranging from 71 nm to 112 nm. It is found that the belts show almost constant conductivity values with an average of approx. 190 S m^{-1} for widths larger than 80 nm. However, when the widths of the belts are reduced below 80 nm the conductivities rise slightly up to approximately 300 S m^{-1} (at 56 nm). These findings are in agreement with prior experiments that were carried out by Jiang *et al.*[26] where single Ppy nanobelts were written and prepared under the same conditions described here. In Jiang's work, the experimental setup provided an electrical connection of the polymer belts with both ends to two macroscopic gold electrodes. For the characterization of electronic transport two metallic needles were then positioned on each of the electrodes and subsequently, current–voltage curves (*I–V* curves) were obtained. The Ppy belts exhibit an enhanced conductivity for belts with a decreased width.[26] Furthermore, it was observed that the conductivity increases sharply when the width of the wires fell below a threshold of 80 nm whereas thicker belts of 100 nm or more show a conductivity of a flat Ppy film (2080 S m^{-1}). For 40 nm wide belts the conductivity increases strikingly by roughly two orders of magnitude (3.2×10^5 S m^{-1} at 10 V).[26] Although the belts were prepared under the same conditions the conductivities measured by means of *I–V*-characteristics and C-AFM experiments exhibit varying values. The differences can be explained as follows: (1) the high conductivities reported by Jiang *et al.*[26] were only observable for high voltages (at 10 V). At a bias voltage of 1 V which would be comparable with the bias voltage used in the C-AFM experiments, a conductivity of 9600 S m^{-1} for a 60 nm wide belt can be estimated, roughly one order of magnitude greater than a 56 nm belt measured in the C-AFM mode. Furthermore, the C-AFM measurements are affected by an additional size-dependent effect which may diminish the charge carrier transport within the polymer belts, as described in the following. In the experiments, we observed the increase in the contact resistance values (determined by analyzing the *y*-intercepts of the resistance *vs.* length curves) for decreasing width of the nano belts (Fig. 3 (top)).

It is reported in the literature that the conduction behaviour of polymeric nanowires is strongly influenced by their morphological architecture.[27] In this study the authors claim that such a kind of nanowires is separated in two different sections: a surface layer with highly-ordered polymer chains and an inner section with the disordered material (Fig. 3 (top), insets). In this context the degree of orientation of the material is equivalent to the electrical conduction properties.[28–30] To account for this, the surface layer is highly conductive whereas the electron transport inside the wire is driven by local defects based on its disordered chain structure. Consequently, a reduction of the diameter of the polymer wires results in an increased number of highly-ordered chains and, thus, to a proportionately lower number of the disordered material.[27,31] However, scanning in contact mode with a repulsive loading force on

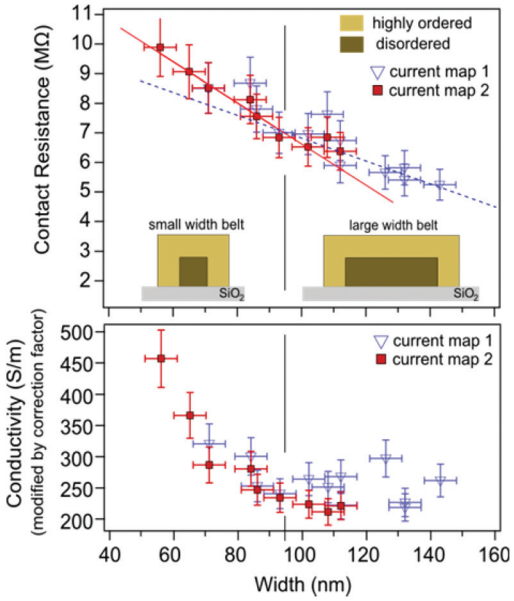

Fig. 3 Contact resistance (top) and modified conductivity (bottom) depending on the width of the polymer belts. The increase of the contact resistance, occurring at the AFM tip–polymer junction, is based on the architecture of decreased, stretched polymers (inset). The vertical lines indicate a transition in the wire architecture. Below a threshold of 90 nm the contact resistance shows a stronger linear increase indicated by different slopes of linear fits (below: red solid, above: blue dashed). Below this point the nanobelts exhibit an enhanced conductivity.

the polymer belts may induce local defects in the highly-ordered layer and consequently led to a diminished conductance efficiency. This leads to the conclusion that C-AFM experiments may affect the measurement itself and influence the electronic properties. Presumably this effect is more pronounced for belts with a reduced width since the acting pressure is spread uniformly on a decreased surface area. Two linear fits to the contact resistance values suggest a transition threshold taking place at a width of roughly 90 nm. The slopes of the fits can be calculated to be $(-6.68 \pm 1.35) \times 10^4$ Ω nm^{-1} (below the threshold, solid red) and $(-3.84 \pm 1.07) \times 10^4$ Ω nm^{-1} for a fit above the threshold (dotted blue). This effect, however, can be factored out by assuming a constant contact resistance in the C-AFM experiments. The linear dependence in the contact resistance allows one to rectify the influence on the conductivity by standardizing to the lowest resistance value. Therefore, each conductivity value was multiplied by correction factors corresponding to the slope of the linear fits. The corrected conductivity values are depicted in Fig. 3 (lower graph). It can be seen that both, the modified conductivities and the contact resistance values, increase at the same point since at this threshold the highly-ordered structure of polymeric wires starts to dominate.[26,27] Although the corrected conductivity values are still lower than that measured with two macroscopic electrodes, the tendency gives a clear hint that one has to consider the influence of force exerted by the AFM tip on the conductivity measurements, especially for soft materials.

Experimental section

Sample preparation: we used electron beam lithography (EBL) for the general preparation of nanobelts, which consists of 5 steps.[20] First of all, gold micro electrodes were fabricated on a thermally oxidized silicon wafer (300 nm) by using a shadow-mask thermal evaporation method (first 2 nm chromium, then 20 nm gold on top). In the next step, the oxidized silicon wafer was modified with a Py-silane (*N*-(3-trimethoxysilylpropyl) pyrrole) monolayer using a vacuum vapor method. Subsequently, the Py-silanized sample surface was spin-coated with a 50 nm thick poly(methylmethacrylate) (PMMA) resist layer. After that, electron beam lithography (EBL) was used to generate a 1D groove pattern into the PMMA layer. Then, the sample was treated with a solution of iron-III-chloride (0.02 M) and pyrrole (0.2 M). The solution was allowed to stand for 15 min to obtain a Py thickness of 25 nm. Finally, after a lift-off process in acetone, the PMMA layer along with the on top coated Ppy were peeled off the substrate. As a result, 1D Ppy nanobelts with a height of 25 nm remain on the gold and SiO_2 surface. The height of the belts is controlled by the reaction time. A more detailed preparation procedure can be found in the work of Jiang *et al.*[26]

Atomic force microscopy: all C-AFM measurements were carried out with a commercial AFM (XE 100, Park Systems Corp., Korea) under ambient conditions operating in contact mode using conductive AFM probes (PPP-ContPt, Nanosensors). The cantilevers have nominal spring constants of 0.2 N m^{-1}. In order to characterize the electrical response of the polymer belts, a bias voltage is applied between the tip and the sample and an external variable gain current amplifier (DHPCA-100, FEMTO Messtechnik GmbH, Germany) is used to measure the current flowing between the tip and the sample during the scanning movement.

Conclusions

In summary, we report quantitative conductivity measurements of polypyrrole belts with different widths ranging from 56 nm to 145 nm. Conductance atomic force microscopy experiments revealed an increase in the conductivity and an increase in the contact resistance with a decreased belt width. The enhanced conductivity is based on highly-ordered polymer chains at the surface. By comparing these results to former experiments we demonstrated that scanning with the AFM tip on the Ppy belts may induce local defects into the highly conductive surface layer and, thus, influence the conductance measurements themselves. Since polypyrrole is a soft material this effect might be considered to be a general effect appearing on soft materials and should be noted. By taking this effect into consideration we calculated a conductivity of roughly 460 S m^{-1} for belts with a width of 56 nm whereas belts with a width above 100 nm exhibited a conductivity of about 250 S m^{-1}. Thus, the findings reported in this work are in good qualitative agreement with the theoretical claims and prior macroscopic conductance experiments we carried out.

Acknowledgements

This work was financially supported by the National Science Foundation of China (NSFC) and Deutsche Forschungsgemeinschaft (DFG) through national projects (91227201 and 21373144) and the Transregional collaborative research center TRR 61. This is also a project supported by the Natural Science Foundation of Jiangsu Province (Project Code, BK20130287), and a project funded by the Collaborative Innovation Center of Suzhou Nano Science & Technology and the Priority Academic Program Development of Jiangsu Higher Education Institutions.

Notes and references

1 G. Binnig, C. F. Quate and C. Gerber, *Phys. Rev. Lett.*, 1986, **56**, 930–933.
2 S. M. Flores and J. L. Toca-Herrera, *Nanoscale*, 2009, **1**, 40–49.
3 S. W. W. Chen, M. Odorico, M. Meillan, L. Vellutini, J. M. Teulon, P. Parot, B. Bennetau and J. L. Pellequer, *Nanoscale*, 2013, **5**, 10877–10886.
4 L. F. Chi, M. Anders, H. Fuchs, R. R. Johnston and H. Ringsdorf, *Science*, 1993, **259**, 213–216.
5 L. F. Chi, H. Fuchs, R. R. Johnston and H. Ringsdorf, *Thin Solid Films*, 1994, **242**, 151–156.
6 S. Holdcroft, *Adv. Mater.*, 2001, **13**, 1753–1765.
7 K. Ramanathan, M. A. Bangar, M. H. Yun, W. F. Chen, A. Mulchandani and N. V. Myung, *Nano Lett.*, 2004, **4**, 1237–1239.
8 A. Mulchandani and N. V. Myung, *Curr. Opin. Biotechnol.*, 2011, **22**, 502–508.
9 J. H. Burroughes, D. D. C. Bradley, A. R. Brown, R. N. Marks, K. Mackay, R. H. Friend, P. L. Burn and A. B. Holmes, *Nature*, 1990, **348**, 352–352.
10 Z. N. Bao, Y. Feng, A. Dodabalapur, V. R. Raju and A. J. Lovinger, *Chem. Mater.*, 1997, **9**, 1299–1301.
11 M. Angelopoulos, *IBM J. Res. Dev.*, 2001, **45**, 57–75.
12 A. S. Arico, P. Bruce, B. Scrosati, J. M. Tarascon and W. Van Schalkwijk, *Nat. Mater.*, 2005, **4**, 366–377.
13 B. Dong, D. Y. Zhong, L. F. Chi and H. Fuchs, *Adv. Mater.*, 2005, **17**, 2736–2741.
14 L. Jiang, X. Wang and L. F. Chi, *Small*, 2011, **7**, 1309–1321.
15 D. Moerman, N. Sebaihi, S. E. Kaviyil, P. Leclere, R. Lazzaroni and O. Douheret, *Nanoscale*, 2014, **6**, 10596–10603.
16 D. Y. Tu, S. Pagliara, A. Camposeo, L. Persano, R. Cingolani and D. Pisignano, *Nanoscale*, 2010, **2**, 2217–2222.
17 T. Kim, S. J. Yang, S. K. Kim, H. S. Choi and C. R. Park, *Nanoscale*, 2014, **6**, 2847–2854.

18 C. Hermosa, J. V. Alvarez, M. R. Azani, C. J. Gomez-Garcia, M. Fritz, J. M. Soler, J. Gomez-Herrero, C. Gomez-Navarro and F. Zamora, *Nat. Commun.*, 2013, **4**, 1709.
19 H. D. Tran, D. Li and R. B. Kaner, *Adv. Mater.*, 2009, **21**, 1487–1499.
20 Y. N. Xia, P. D. Yang, Y. G. Sun, Y. Y. Wu, B. Mayers, B. Gates, Y. D. Yin, F. Kim and Y. Q. Yan, *Adv. Mater.*, 2003, **15**, 353–389.
21 H. J. Dai, E. W. Wong and C. M. Lieber, *Science*, 1996, **272**, 523–526.
22 P. J. de Pablo, C. Gomez-Navarro, J. Colchero, P. A. Serena, J. Gomez-Herrero and A. M. Baro, *Phys. Rev. Lett.*, 2002, **88**, 036804.
23 C. Gomez-Navarro, P. J. de Pablo and J. Gomez-Herrero, *J. Mater. Sci. Mater. Electron.*, 2006, **17**, 475–482.
24 S. Sengupta, D. Ebeling, S. Patwardhan, X. Zhang, H. von Berlepsch, C. Bottcher, V. Stepanenko, S. Uemura, C. Hentschel, H. Fuchs, F. C. Grozema, L. D. A. Siebbeles, A. R. Holzwarth, L. F. Chi and F. Wurthner, *Angew. Chem., Int. Ed.*, 2012, **51**, 6378–6382.
25 V. V. Zagorsky, V. E. Bochenkov, S. V. Ivashko and G. B. Sergeev, *Mater. Sci. Eng., C*, 1999, **8–9**, 329–334.
26 L. Jiang, Y. H. Sun, H. Y. Peng, L.-J. Li, T. Wu, J. Ma, F. Y. C. Boey, X. D. Chen and L. F. Chi, *Small*, 2011, **7**, 1949–1953.
27 C. R. Martin, *Acc. Chem. Res.*, 1995, **28**, 61–68.
28 H. X. He, C. Z. Li and N. J. Tao, *Appl. Phys. Lett.*, 2001, **78**, 811–813.
29 L. Abell, P. N. Adams and A. P. Monkman, *Polymer*, 1996, **37**, 5927–5931.
30 H. M. Xiao, W. D. Zhang, C. Lv, S. Y. Fu, M. X. Wan and Y. W. Mai, *Macromol. Chem. Phys.*, 2010, **211**, 1109–1116.
31 M. X. Wan, M. Li, X. Mi, Q. Jiang and P. X. Ye, *Chin. J. Polym. Sci.*, 1996, **14**, 80–85.